https://doi.org/10.5194/tc-2019-329
Preprint. Discussion started: 14 January 2020

The Cryosphere Discussions

Sensitivity of Greenland ice sheet projections to spatial resolution in higher-order simulations: the AWI contribution to ISMIP6-Greenland using ISSM

Martin Rückamp[1], Heiko Goelzer[2,3], and Angelika Humbert[1,4]

[1]Alfred-Wegener-Institut Helmholtz-Zentrum für Polar- und Meeresforschung, Bremerhaven, Germany
[2]Utrecht University, Institute for Marine and Atmospheric Research (IMAU), Utrecht, the Netherlands
[3]Laboratoire de Glaciologie, Université Libre de Bruxelles, Brussels, Belgium
[4]University of Bremen, Bremen, Germany

Correspondence: Martin Rückamp (martin.rueckamp@awi.de)

Abstract. Projections of the contribution of the Greenland ice sheet to future sea-level rise include uncertainties primarily due to the imposed climate forcing and the initial state of the ice sheet model. Several state-of-the-art ice flow models are currently being employed on various grid resolutions to estimate future mass changes in the framework of the Ice Sheet Model Intercomparison Project for CMIP6 (ISMIP6). Here we investigate the sensitivity to grid resolution on centennial sea-level contributions from the Greenland ice sheet and study the mechanism at play. To this end, we employ the finite-element higher-order ice flow model ISSM and conduct experiments with four different horizontal resolutions, namely 4, 2, 1 and 0.75 km. We run the simulation based on the ISMIP6 core GCM MIROC5 under the high emission scenario RCP8.5 and consider both atmospheric and oceanic forcing in full and separate scenarios. Under the full scenarios, finer simulations unveil up to $\sim$5% more sea-level rise compared to the coarser resolution. The sensitivity depends on the magnitude of outlet glacier retreat, which is implemented as a series of retreat masks following the ISMIP6 protocol. Without imposed retreat under atmosphere-only forcing, the resolution dependency exhibits an opposite behaviour with about $\sim$5% more sea-level contribution in the coarser resolution. The sea-level contribution indicates a converging behaviour $\leq 1\,\mathrm{km}$ horizontal resolution. A driving mechanism for differences is the ability to resolve the bed topography, which highly controls ice discharge to the ocean. Additionally, thinning and acceleration emerge to propagate further inland in high resolution for many glaciers. A major response mechanism is sliding (despite no climate-induced hydrological feedback is invoked), with an enhanced feedback on the effective normal pressure N at higher resolution leading to a larger increase in sliding speeds under scenarios with outlet glacier retreat.

1 Introduction

Climate change is the major driver of global sea-level rise (SLR), which has been shown to accelerate (Nerem et al., 2018; Shepherd et al., 2019). The Greenland ice sheet (GrIS) has contributed about 20% to sea-level rise during the last decade

https://doi.org/10.5194/tc-2019-329
Preprint. Discussion started: 14 January 2020

(Rietbroek et al., 2016). Holding in total an ice mass of ∼7.42 m sea-level equivalent (SLE) (Morlighem et al., 2017), its future contribution poses a major societal challenge. Since 1992, the GrIS mass loss is controlled on average at 52% by surface mass balance (SMB), with the remainder of 48% being due to increased ice discharge of outlet glaciers into the surrounding ocean (Shepherd et al., 2019).

While the relative importance of outlet glacier discharge for total GrIS mass loss has decreased since 2001 (Enderlin et al., 2014; Mouginot et al., 2019) and is expected to decrease further in the future (e.g. Aschwanden et al., 2019), it remains an important aspect for projecting future sea-level contributions from the ice sheet on the centennial timescale. (Goelzer et al., 2013; Fürst et al., 2015). A (non-linear) dynamic response of the ice sheet is caused by changes in the atmospheric and oceanic forcing, that may trigger glacier acceleration and thinning of outlet glaciers. Moreover, processes such as SMB and ice discharge are mutually competitive in removing mass from the ice sheet (Goelzer et al., 2013; Fürst et al., 2015). Beside this interplay, a simple extrapolation of observed GrIS mass loss trends over the next century is not justified, as high temporal variations in SMB and glacier acceleration are apparent (e.g. Moon et al., 2012). Therefore, reliable ice sheet models (ISMs) forced with future climate data must be driven for policy relevant sea-level projections on century time scales.

The Ice Sheet Model Intercomparison Project (ISMIP6, Nowicki et al., 2016) is an international community effort striving to improve sea-level projections from the Greenland and Antarctic ice sheets. Based on previous efforts like SeaRISE (Bindschadler et al., 2013; Nowicki et al., 2013) and ice2sea (e.g., Gillet-Chaulet et al., 2012), ISMIP6 continues to fully explore the sea-level rise contribution and associated uncertainties. The effort is aligned with the Coupled Model Intercomparison Project Phase 6 (CMIP6, Eyring et al., 2016) to provide input for the upcoming assessment report of the Intergovernmental Panel on Climate Change (IPCC AR6).

Despite substantial progress in ice sheet modelling in the last decades and years, a challenging goal remains to narrow uncertainties and improve reliability of future sea-level projections from the two big ice sheets. Up to date, it is recognized that the largest uncertainty sources are related to the initialization of the ISM or stem from the external forcing (Goelzer et al., 2020).

The first ISMIP6 project initMIP-Greenland (Goelzer et al., 2018) particularly targeting the initialization techniques used in the ice sheet modelling community. The schematic forward experiment was not designed to estimate realistic sea-level contribution, but it provides valuable insights how the initial state of an ISM affect the ice sheet response. Under a predefined SMB anomaly, mass losses reveal a large spread. Although the spread is attributed to the large diversity in model approaches, initMIP-Greenland shows notable improvements (e.g., a reduced model drift) and more consistent results compared to earlier large scale intercomparison exercises.

The results of the initMIP exercise are certainly affected by other not obvious factors than the initialization. Interestingly, the estimated sea-level contributions show barely a dependence on grid resolution (Fig. 1). ISM versions with multiple grid resolutions demonstrate that coarser grid resolutions tend to produce a slightly larger mass loss. This effect is partly due to the methodological approach by considering a SMB anomaly that is based on the present-day observed SMB. Therefore, coarse resolution models not rendering the present-day ice margin perfectly well likely overestimate ablation.

https://doi.org/10.5194/tc-2019-329
Preprint. Discussion started: 14 January 2020

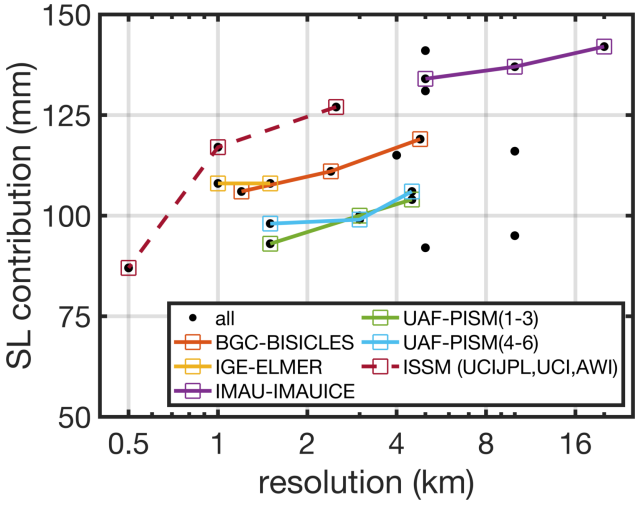

Figure 1. Results from the initMIP-Greenland exercise (Goelzer et al., 2018). Sea-level contribution versus (minimum) horizontal grid resolution of each participating ISM. Equal model versions but different grid resolutions are connected with a coloured line. ISSM model versions are connected with a coloured dashed line. Note the logarithmic scale of the x-axis.

Greve and Herzfeld (2013) explored how spatial grid resolutions of 20, 10, and 5 km impact the ice mass change under standardized future climate scenarios. The simulations demonstrated that the absolute ice volumes in the initial state depend significantly on the resolution; the 5 km resolution setup holds a SLE that is approx. 0.1 m lower than the 20 km resolution setup. However, the sensitivities in the forward experiments vary only by a few percents and do not show a consistent trend among all conducted experiments. A limitation of this study is the employed SIA approximation, which is known to be invalid for fast-flowing outlet glaciers, and the medium to coarse resolution range which is insufficient to resolve the narrow and confined outlet glaciers in Greenland correctly.

Aschwanden et al. (2016) highlighted the importance of grid resolution on GrIS flow behaviour by accurately resolving the ice geometry. Their result indicates, that a resolution of $< 1\,\mathrm{km}$ is required to replicate the overall flow pattern without spatially tuning relevant parameters. In a subsequent study, Aschwanden et al. (2019) performed large-scale GrIS projections on millennial time scales under RCP 2.6, 4.5 and 8.5 scenarios. Besides their ensemble predictions, they present individual grid-dependent simulations (ranging from 0.6 to 18 km) (simulations G600-G18000 in Tab. 1 in Aschwanden et al., 2019). There is no clear trend in the sea-level contribution as a function of grid resolution identifiable. The simulation with a grid spacing of 1800 m tends to produce the largest sea-level contribution compared to the other resolutions. Ice discharge (consists in Aschwanden et al. (2019) as the sum of mechanical calving and frontal melt) for grid resolutions 1800 m and smaller are very similar and likely will not change significantly under further grid refinement; however, the SMB still lowers when the resolution increases (pers. comm. A. Aschwanden). Their study is based on shallow ice approximation, including shallow shelf approximation for sliding.

https://doi.org/10.5194/tc-2019-329
Preprint. Discussion started: 14 January 2020

Increasing the spatial resolution comes along with the ability to resolve the geometry and to track outlet glacier behavior which is a prerequisite formulated by the IPCC (Church et al., 2013) to improve projections. In turn, it requires a larger amount of computational resources. To identify an acceptable limit in spatial resolution would be valuable to balance computational amount, data storage and particularly to make progress in narrowing uncertainties in ice sheet projections, even if only by a few percent. The adequate resolution is also depending on the approximation of the momentum balance. For capturing the dynamics of outlet glaciers, higher-order approximation is providing a suitable physical basis and is therefore chosen for this study.

The current ISMIP6-projection-Greenland multi-ensemble effort analyse the future sea-level contribution from various ISMs (Goelzer et al., 2020). Though the exercise shows that models with low and high resolution are found at the upper and lower bound of sea-level contribution, no specific analysis to this task is performed. Therefore, the main intention of this paper is to evaluate the sensitivity of the simulated GrIS response to global warming due to different horizontal grid resolutions by one single ISM.

To this end, the Ice Sheet System Model (ISSM, Larour et al., 2012) is applied to the GrIS with the higher-order Blatter-Pattyn-type approximation and resolutions ranging from medium to high (4 and 0.75 km at fast flowing outlet glaciers, respectively). For comparison, the resolutions covered by the ISMs in the ISMIP6-projection-Greenland exercise ranges between 0.25 km (JPL-ISSM) and 16 km (IMAU-IMAUICE1). Simulations are forced by climate data from the CMIP5 global circulation model (GCM) MIROC5 under the Representative Concentration Pathway (RCP, Moss et al., 2010) 8.5 following the ISMIP6 protocol (Nowicki et al., 2020b). A secondary aim of this paper is to describe in detail how the ISMIP6 exercise has been conducted using ISSM, which could be valuable for a broader audience[1].

2 Ice flow model ISSM

The model applied here is the Ice Sheet System Model (ISSM, Larour et al., 2012). It has been applied successfully to the GrIS in the past (Seroussi et al., 2013; Goelzer et al., 2018; Rückamp et al., 2018, 2019a) and is also used for studies of individual drainage basins of Greenland, e.g. the North East Greenland Ice Stream (Choi et al., 2017), Jakobshavn Isbræ (Bondzio et al., 2017) and Petermann Glacier (Rückamp et al., 2019b).

ISSM is designed to use variable ice flow approximations ranging from shallow ice approximation to full-Stokes and has also the capability to perform inverse modelling to constrain unknown parameters. Here, we make use of the Blatter-Pattyn higer-order approximation (BP, Blatter, 1995; Pattyn, 2003) to balance model accuracy and computational costs. The system of equations are solved numerically with the finite element method on an unstructured grid. The latter allows for variable resolution in key areas of the ice sheet, e.g. marine terminating outlet glaciers. State variables are computed on each vertex of the mesh using piecewise-linear finite elements. The ice rheology is treated with a regularized Glen flow law, a temperature-dependent rate factor for cold ice, and a water-content-dependent rate factor for temperate ice.

[1] Although there are various ISSM contributions from different groups with different model characteristics to ISMIP6-projection-Greenland, we will simply use 'ISSM' for the ISMIP6 contribution AWI-ISSM in the following text. At some instances we will use AWI-ISSM to avoid any misunderstanding.

https://doi.org/10.5194/tc-2019-329
Preprint. Discussion started: 14 January 2020

At the ice base sliding is allowed everywhere and the basal drag, τ_{b}, is written as

$$\tau_{\mathrm{b},i} = -k^2 N v_{\mathrm{b},i}, \tag{1}$$

where $v_{\mathrm{b},i}$ is the basal velocity vector in the horizontal plane and $i = x, y$. The friction coefficient k^2 is assumed to cover bed properties such as bed roughness. Here, k^2 is retrieved by an inversion technique (see sect. 3.1). The effective pressure is defined as $N = \varrho_i\, g\, h + \min(0, \varrho_{\mathrm{w}}\, g\, z_{\mathrm{b}})$, where h is the ice thickness, z_{b} the glacier base and $\varrho_i = 910\,\mathrm{kg\,m^{-3}}$, $\varrho_w = 1028\,\mathrm{kg\,m^{-3}}$ the densities for ice and sea water, respectively. At lateral boundaries water pressure is applied at marine terminating glaciers and zero pressure along land terminating ice cliffs. A traction-free boundary condition is imposed at the ice/air interface.

The ISSM model domain for the Greenland ice sheet covers the present-day main ice sheet extent on the EPSG:3413 grid, and includes the current floating ice tongues (e.g., Petermann, Ryder and 79° North glaciers). The geometric input is BedMachine v3 (Morlighem et al., 2017). Thickness, bedrock and ice sheet mask is clipped to exclude glaciers and ice caps surrounding the ice sheet proper. The initial ice sheet mask is manually retrieved from the data coverage of the MEaSURE velocity dataset (Joughin et al., 2010, 2016) to ensure an available target for the employed basal friction inversion (see below). A minimum ice thickness of 1 m is applied. Grounding line evolution is treated with a sub-grid parameterization scheme, which tracks the grounding line position within the element (Seroussi et al., 2014). A sub-grid parameterization on partially floating elements for basal melt is applied (Seroussi and Morlighem, 2018). The basal melt rate below floating tongues is parameterized with a Beckmann–Goosse relationship (Beckmann and Goosse, 2003). The melt factor is roughly adjusted such that melting rates correspond to literature values (e.g. Wilson et al., 2017; Rückamp et al., 2019b). In this parameterization ocean temperature and salinity are set to -1.7°C and 35 Psu, respectively.

Model calculations with ISSM are performed on a horizontally unstructured grid. To limit the number of elements while maximizing the horizontal resolution in regions where physics demands higher accuracy, the horizontal mesh is generated with a higher resolution of $\mathrm{RES}_{\mathrm{min}}$ in fast-flowing regions (observed ice velocity $> 200\,\mathrm{m\,a^{-1}}$) and a coarser resolution of $\mathrm{RES}_{\mathrm{max}}$ in the interior. Experiments are carried out at four different horizontal grid resolutions with $\mathrm{RES}_{\mathrm{min}}$ equal to 4, 2, 1, and 0.75 km (Tab. 1 and Fig. 2). The experiments G1000 and G750 are a contribution to the ISMIP6 ensemble, termed AWI-ISSM2 and AWI-ISSM3 in Goelzer et al. (2020), respectively. Additionally, we contributed with AWI-ISSM1 to ISMIP6, but this model version is neglected here as its has an alternative meshing approach and is therefore not directly comparable.

The distribution of mesh vertices at numerous outlet glaciers is depicted in Figs. S3 to S16. The horizontal resolution of a triangle is defined by its minimum edge length. Independent of the horizontal resolution, the vertical discretization comprises 15 terrain-following layers, refined towards the base where vertical shearing becomes more important.

During all transient runs, we neglect an evolution of the thermal field. This is justified as it was shown by Seroussi et al. (2013) and Goelzer et al. (2018, see submissions AWI-ISSM1 and 2) that the temperature field and its change has a negligible effect on century time-scale projections of the GrIS.

https://doi.org/10.5194/tc-2019-329
Preprint. Discussion started: 14 January 2020

The Cryosphere Discussions
Open Access
EGU

Table 1. Summary of models and their mesh characteristics. Computational time is based on a projection run under MIROC5 RCP 8.5 and medium ocean forcing.

Model name (this study)	Model name (ISMIP6)	$\mathrm{RES}_{\mathrm{min}}$ (km)	$\mathrm{RES}_{\mathrm{max}}$ (km)	number of elements	time step Δt (yr)	computational time (minutes)	number of cores
G4000	-	4	7.5	1 169 546	0.100	83	90*
G2000	-	2	7.5	1 951 586	0.050	252	162*
G1000	AWI-ISSM2	1	7.5	4 241 020	0.025	640	342†
G750	AWI-ISSM3	0.75	7.5	6 220 928	0.010	1731	702†

* Intel Xeon Broadwell CPU E5-2697 v4, 2.3 GHz on the AWI HPC system Cray CS400.
† Intel Xeon Broadwell CPU E5-2695 v4, 2.1 GHz on the DKRZ HPC system Mistral.

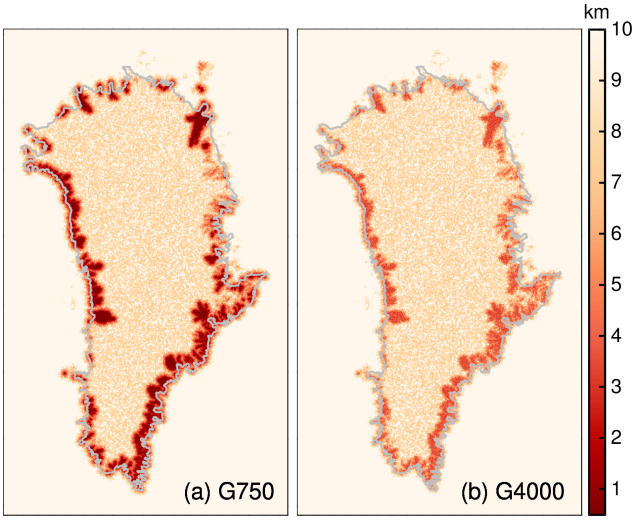

Figure 2. Horizontal mesh resolution (in km) used for G750 (a) and G8000 (b). Data are clipped at 0.5 and 10 km. The horizontal resolution of a triangle is defined by its minimum edge length. The grey line delineates the ice domain from the initialization.

3 ISMIP6 experimental design

It is beyond the scope of this paper to present the details of the ISMIP6 protocol and experimental design. Therefore, we aim to briefly outline the external forcing approach. Further details are given in Goelzer et al. (2020), Nowicki et al. (2020a), Fettweis et al. (2020), Slater et al. (2019a) and Slater et al. (2019b).

The experimental design for the ISMIP6 projections is based on the precursor initMIP-Greenland (Goelzer et al., 2018), which studied the model initialization techniques used in the ice sheet modelling community. For the ISMIP6-Greenland projections groups were asked to participate with their already existing or improved initMIP setup. As the ISMIP6 philosophy follows the "come as you are" approach each model involved has different flavours in model characteristics and probably in the

https://doi.org/10.5194/tc-2019-329
Preprint. Discussion started: 14 January 2020

assigned reference year. Therefore, in a series of experiments, the first ISMIP6 experiment, termed historical, is dedicated to bring each model to the common ISMIP6 start date at end of 2014 from where on the future climate scenarios branch off. Given the fact that every model initialization has its own evolving response to a prescribed experiment, an unforced constant-climate control experiment is defined to capture the model drift with respect to the ISM reference climate.

The set of experiments can be summarized as follows:

- initialization: experiment to retrieve the initial state of the model.
- control: experiment where the climate is held constant to the reference climate (lasts until end of December 2100).
- historical: experiment to bring model from the initialization state to ISMIP6 projection start date (lasts until end of December 2014).
- projection: future climate scenario (from January 2015 to end of December 2100).

We aim to study the effect of grid resolution on ice mass changes. Therefore, we selected the MIROC5 under RCP8.5 climate which is a core experiment in ISMIP6. The GCM MIROC5 was selected as it performs well in the historical period and represents a plausible climate near Greenland (Barthel et al., 2019). The ensemble projections will be explored in separate papers by Goelzer et al. (2020) and Nowicki et al. (2020a).

Conducted projection experiments and the corresponding experiment labels used in this study are summarized in Tab. 2. In the ISMIP6 ensemble study, the experiments with low, medium, and high oceanic forcing (explained below) are needed to quantify related uncertainties. Here, we run MIROC5 RCP8.5 with low, medium and high oceanic forcing as we expect increasing ice discharge with larger retreat of outlet glaciers. Thus, they can be interpreted as a weighting between the competing tendencies of SMB and ice discharge. If both external forcings are considered the scenarios are termed as 'full' in the following. In addition we perform simulations where only the atmospheric forcing (RCP8.5-Rnone) or only tidewater glacier retreat (OO-Rmed/high) is at play. The RCP8.5-Rnone and OO-Rmed/high experiments are consequently a setup to explore the impact of SMB and ice discharge on mass loss separately.

Please note, that for the presented study more experiments (e.g., atmospheric only) from extended model versions (larger range of horizontal resolutions) are performed other than available in the ISMIP6-projection-Greenland exercise.

3.1 Initialization

The initialization state of ISSM is based on inversion for determining the basal friction coefficient. Before the inversion, a relaxation run assuming no sliding and a constant ice temperature of $-10°C$ is performed to avoid spurious noise that arises from errors and biases in the datasets. To ensure that the relaxed geometry does not deviate too much from the observed geometry, the relaxation is conducted over one year. However, while inverse modelling is well established for estimating basal properties, the temperature field is difficult to constrain without performing an interglacial thermal spin-up. Therefore, we rely on a temperature field that was obtained by a hybrid approach between paleoclimatic thermal spin-up and basal friction inversion. This method was developed for the AWI contribution in initMIP-Greenland (Goelzer et al., 2018) and

https://doi.org/10.5194/tc-2019-329
Preprint. Discussion started: 14 January 2020

Table 2. Summary of projection experiments based on MIROC5-RCP8.5 climate data.

Experiment label	atmospheric forcing	oceanic forcing
RCP8.5-Rlow	SMB anomaly	low
RCP8.5-Rmed	SMB anomaly	med
RCP8.5-Rhigh	SMB anomaly	high
RCP8.5-Rnone	SMB anomaly	-
OO-Rmed	-	med
OO-Rhigh	-	high

further improved in Rückamp et al. (2018) by using the geothermal flux pattern from Greve (2005, scenario hf-pmod2). Here, we initialize the ice rheology by interpolating the 3D temperature and watercontent fields from the hybrid spin-up in Rückamp et al. (2018) on the ISSM grid. Equivalent we interpolate the basal melt rates of grounded ice.

The inversion approach infers the basal friction coefficient k^2 in Eq. 1 by minimizing a cost function that measures the misfit between observed and modelled horizontal velocities (Morlighem et al., 2010). The cost function is composed of two terms which fit the velocities in fast- and slow-moving areas. A third term is a Tikhonov regularization to avoid oscillations. The parameters for weighting the three contributions to the cost function are taken from Seroussi et al. (2013). We leverage horizontal surface velocities from the MEaSURE project (Joughin et al., 2010, 2016), as the dataset with almost no gaps over GrIS is suitable for basal friction inversion.

The assigned reference year is 1990. This date is not in agreement with the timestamps of the BedMachine dataset (reference time is 2007) and the MEaSURE velocity dataset (temporal coverage from 2014 to 2018). However, we ignore the contemporaneity requirement in the inversion approach and place more value on to start the projections at the end of the assumed GrIS steady-state period (e.g. Ettema et al., 2009).

3.2 Historical scenario

To bring our model from the reference time to the projection start date, the historical scenario is needed. During the historical period, yearly cumulative SMB is taken from the RACMO2.3p2 product (Noël et al., 2018) for the years from 1990 to 2015. In this scenario the ice front is fixed in time. That means calving exactly compensates the outflow through the margins, and initially glaciated points are not allowed to become ice-free.

3.3 Future climate scenarios

3.3.1 Atmospheric forcing

ISMIP6 provide surface forcing datasets for the GrIS based on CMIP GCM simulations. The GCM output is dynamically downscaled through the higher-resolution regional climate model (RCM) MAR v3.9 (Fettweis et al., 2017). The latter allows

https://doi.org/10.5194/tc-2019-329
Preprint. Discussion started: 14 January 2020

to capture narrow regions at the periphery of the Greenland ice sheet with large SMB gradients, which are likely not captured by the GCMs. The climatic SMB that is used as future climate forcing reads

$$\mathrm{SMB_{clim}}(x,y,t) = \mathrm{SMB_{ref}}(x,y) + \Delta\mathrm{SMB}(x,y,t) + \mathrm{SMB_{dyn}}(x,y,t), \tag{2}$$

with the anomaly defined as

$$\Delta\mathrm{SMB}(x,y,t) = \mathrm{SMB}(x,y,t)_{\mathrm{GCM-MAR}} - \overline{\mathrm{SMB}}(x,y)^{1960-1989}_{\mathrm{GCM-MAR}}, \tag{3}$$

where $\mathrm{SMB}(x,y,t)_{\mathrm{GCM-MAR}}$ is the direct output of MAR using the GCM climate data and $\overline{\mathrm{SMB}}(x,y)^{1960-1989}_{\mathrm{GCM-MAR}}$ the corresponding mean value over the reference period (from January 1960 to December 1989). As the reference SMB field $\mathrm{SMB_{ref}}(x,y)$, we choose the downscaled RACMO2.3p2 product (Noël et al., 2018) whereby a model output was averaged for the period 1960–1990. This period is chosen as the ice sheet is assumed close to steady-state in this period. (e.g. Ettema et al., 2009). The SMB deduced by MAR is processed on a fixed topography (off-line), consequently local climate feedback processes due to the evolving surface in the projection experiments are not captured. The SMB height-elevation feedback is considered with a dynamic correction $\mathrm{SMB_{dyn}}$ to the $\mathrm{SMB_{clim}}$ following Franco et al. (2012)

$$\mathrm{SMB_{dyn}}(x,y,t) = \mathrm{dSMBdz(x,y,t)} \times (z_s(x,y,t) - z_{\mathrm{ref}}(x,y)). \tag{4}$$

The surface elevation changes are taken from the ISM elevation $z_s(x,y,t)$ while running the simulation and the corresponding ISM reference elevation $z_{\mathrm{ref}}(x,y)$ from the initialization state. The yearly patterns of $\Delta\mathrm{SMB}(x,y,t)$ and $\mathrm{dSMBdz}(x,y,t)$ are provided by ISMIP6. A cumulative SMB anomaly over the projection period is shown in Fig. 3a.

3.3.2 Oceanic forcing

Different strategies for oceanic forcing are part of the ISMIP6 protocol. Here, we rely on the standard approach which is an empirically-derived, sector averaged calving front retreat as a function of climate forcing. In this approach, the oceanic forcing is translated into an outlet glacier retreat parametrization (Slater et al., 2019a, b). It parameterizes calving front retreat as a function of projected submarine melting (taking into account changes in ocean temperature and surface meltwater runoff from a GCM). The parametrization is not applied to the individual glaciers but over a predefined geographical region. Based on the numerous retreat trajectories a medium retreat scenario as the trajectory with the median retreat at 2100 is defined. To cover uncertainty by this approach a low and high retreat scenarios is defined as the trajectories with the 25th and 75th percentile retreats at 2100.

Result in the retreat is up to 15 km by 2100 in RCP8.5-Rmed scenario (Slater et al., 2019a). The retreat mask for RCP8.5-Rhigh in 2100 is exemplary shown in Fig. 3b. Please note, that within this method, the calving front retreat is directly prescribed and no longer a response of the ISM (i.e., not a result of ice velocity at calving front, calving rate and frontal melt). The imposed retreat is therefore a composition of ice discharge, calving and frontal melt.

The ISMIP6 protocol recommends using a sub-grid scheme to simulate fractional retreat in a grid cell for coarse resolution models. The ISMIP6 AWI-ISSM contribution are performed without fractional retreat, and therefore the additional conducted

https://doi.org/10.5194/tc-2019-329
Preprint. Discussion started: 14 January 2020

The Cryosphere Discussions
Open Access
EGU

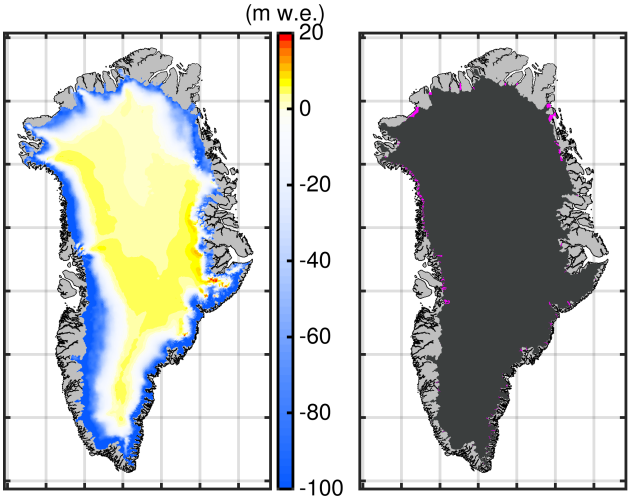

Figure 3. Atmospheric and oceanic forcing. (a) Spatial pattern of the cumulative (2015–2100) SMB anomaly based on MIROC5-RCP8.5 and downscaled with MAR (Fettweis et al., 2020). (b) Retreat of tidewater glaciers under RCP8.5-Rhigh scenario. Purple areas indicate retreated areas in 2100.

simulations in this study equivalently do not use a sub-grid scheme. This enables a consistent comparison between the different grids and test their sensitivity to grid resolution. Moreover, a sub-grid scheme would mimic a higher resolution which is not wanted here. However, the binary retreat masks (i.e. ice and non-ice covered cells) are interpolated to the native grid by nearest neighbour interpolation. Retreat occurs once a cell is fully emptied.

4 Results

Before presenting the results, we aim to address the terminology used for clarity. Following the glossary in Cogley et al. (2011), ice discharge is computed as the product of ice thickness h and the depth-averaged velocity $\bar{v}$. In the following, the lower-case q refers to the local ice discharge at a point, and the upper-case Q refers to the glacier-wide quantity (analogous for other quantities such as glacier-wide calving D and local calving d). Quantities at the margin are reckoned in the normal direction.

4.1 Initial state

To evaluate the modelling decisions pertaining the initialization, the state of the ice sheet at the end of the historical period is compared to observations. Due to the sparseness and limited temporal and spatial coverage of available observations, we rely on the BedMachine v3 (150 m grid spacing) and MEaSURE datasets (250 m grid spacing) for ice thickness and surface velocity, respectively. As these data are used in the data assimilation and inversion, velocity and thickness are not independent quantities. However, during the historical period the ice sheet state is altered by the boundary conditions and external forcing.

https://doi.org/10.5194/tc-2019-329
Preprint. Discussion started: 14 January 2020

Therefore, the following evaluation attempts to quantify differences from the model configurations at the ISMIP6 projection start date.

Since the results are qualitatively similar for each grid simulation, the surface velocity field of the G750 simulation is exemplarily shown in Fig. 4a. A consequence of the employed basal friction inversion is the high fidelity in simulating the observed velocity field (not shown). The evaluation to observed velocities is shown in Fig. 4b. With increasing spatial resolution, the root mean square error (RMSE) decreases. However, the ice sheet-wide RMSE of each model version is very similar but in the areas of fast-flowing outlet glaciers (observed velocity $> 200\,\mathrm{m\,a^{-1}}$) differences are more evident: The G4000 and G750 simulations yield $\mathrm{RMSE} = 150\,\mathrm{m\,a^{-1}}$ and $\mathrm{RMSE} = 80\,\mathrm{m\,a^{-1}}$, respectively. Note that these values are not identical to those given in Goelzer et al. (2020), as the evaluation here is based on a different subsampling method. A mean signed difference (MSD) reflects an increasing underestimation of the simulated velocities with decreasing resolution. The underestimation of prominent outlet glaciers for the G4000 setup is demonstrated in the spatial pattern of velocity differences in Fig. S1. With increasing resolution, the difference pattern becomes more heterogeneous. Although barely visible, the G750 setup provides an interesting signature at narrowly confined outlet glaciers: Generally, the velocities in the main trunk are underestimated while beneath the shear margin velocities are overestimated. This is due to the fact, that the employed resolution is not able to resolve the sharp velocity jump across the shear margin.

A similar evaluation for the thickness is performed. The ice sheet-wide RMSE of ice thickness is shown (Fig. 4c) and depicts the same grid-dependent behaviour as the velocity evaluation. Similarly, the RMSE show larger differences in the fast flow regions: The G4000 and G750 simulations yield $\mathrm{RMSE} = 126\,\mathrm{m}$ and $\mathrm{RMSE} = 45\,\mathrm{m}$, respectively. In this region, the MSD indicates underestimation of ice thicknesses with increasing resolution. Similar as mentioned above, these values are not identical to those given in Goelzer et al. (2020), as the evaluation here is based on a different subsampling method. Spatial patterns of the thickness differences are shown in Fig. S2.

The stored volumes, ice extent and spatially integrated SMB is among all grid simulations similar ($V = 7.28\,\mathrm{m\,SLE} \pm 0.2\%$, $A = 1.787 \times 10^6 \mathrm{km}^2 \pm 0.7\%$, $\mathrm{SMB} = 375\,\mathrm{Gt\,a^{-1}} \pm 0.2\%$). However, the underestimation of velocities and ice thicknesses in the coarser resolution models is confirmed by the temporal mean of the ice discharge in the historical period. The intrinsically simulated ice discharge Q yields $207\,\mathrm{Gt\,a^{-1}}$ to $341\,\mathrm{Gt\,a^{-1}}$ for the G4000 and G750 simulations, respectively. As the ice front is not moving ice discharge Q equals calving D.

4.2 Sea-level contribution

In the following the transient effect of spatial resolution on ice volume evolution for the future-climate experiments is studied. The change in ice mass loss is expressed as sea-level contributions. Therefore, the simulated volume above flotation is converted into the total amount of global sea-level equivalent by assuming a constant ocean area of $3.618 \times 10^8\,\mathrm{km}^2$. For all conducted projection experiments, the determined GrIS mass losses as a function of time are shown in Fig. 6. The mass losses in the projection experiments are corrected with the control run with respect to the reference time.

In the constant climate control experiment, the model response in the absence of additional forcing is evaluated (thin coloured lines in Fig. 6). The transient response should not be interpreted as a prediction of actual future behaviour, the control run

https://doi.org/10.5194/tc-2019-329
Preprint. Discussion started: 14 January 2020

The Cryosphere Discussions
Open Access
EGU

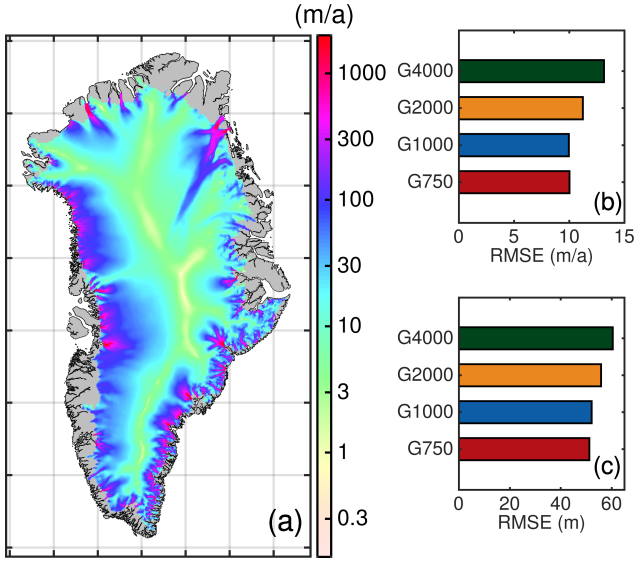

Figure 4. Simulation and error estimate of model output at the end of the historical run compared to observations. (a) Simulated surface velocity of the GrIS ($\mathrm{m\,a^{-1}}$) from the G750 simulation. The grey silhouette shows the Greenland land mask from BedMachine v3. (b) Root mean square error (RMSE) of the horizontal velocity magnitude compared to MEaSURE. (c) RMSE of ice thickness compared to BedMachine v3. The diagnostics have been calculated on the regular MEaSURE and BedMachine grids, respectively.

rather confirms that each model has achieved a high degree of equilibration, which is reflected with a low rate of volume change. The simulated ice mass evolution shows for all models a mass gain for the 111-year control experiment ranging between -28 and -2 mm. With increasing resolution, the drift gets smaller and is minimal for the G1000 and G750 simulation. Although projections are corrected with the control run, the higher drift needs caution when interpreting the results as it has, e.g. a consequence on the SMB height-elevation feedback. The higher mass gain rates of the coarser resolutions in the control simulation are due with the lower ice discharge rates (see above). Although the integrated signal in ice mass change is generally small, the spatial patterns reveal an ice thickness imbalance up to hundreds of metres over the control period (Fig. 5). Imposing a SMB correction to suppress the thickness imbalance would be feasible for maintaining a small drift. However, this is avoided here to enable a clean comparison between the four model version and to leave the ice dynamics some degree of freedom. Moreover, the mass trends represent an important diagnostic. Comparing the ice thickness changes reveal distinct differences between the grid-resolution simulations (Fig. 5). For example, at the end of the control run, at some western and north-western locations at the margin the G4000 simulation exhibit thickening while the G750 reveals thinning. Another example is simulated at the south-western margin, where extensive thickening is prevailing in all simulations but reaches farther inland in the coarser resolutions. However, from these figures, it becomes clear that positive and negative thickness changes partially compensate, resulting in a low model drift.

Depending on the projection scenario, the GrIS will lose ice corresponding to a SLE between 19 mm (or 108 excluding OO-Rmed/high) and 137 mm. For the future climate scenarios including atmospheric forcing a gradual increase in mass loss

https://doi.org/10.5194/tc-2019-329
Preprint. Discussion started: 14 January 2020

The Cryosphere Discussions
Open Access
EGU

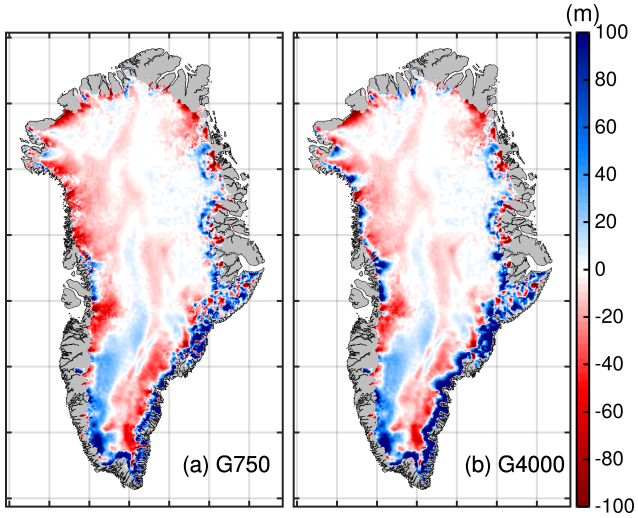

Figure 5. Ice thickness change ($h(t = 2100) - h(t = 2015)$) for the control run. (a) G750 simulation and (b) G4000 simulation. The grey silhouette shows the Greenland land mask from BedMachine v3. Positive values represents thickening, and negative shows thinning.

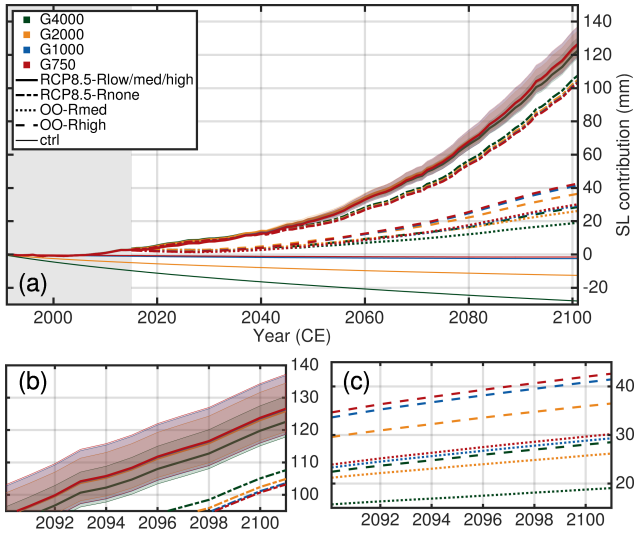

Figure 6. Projected sea-level contribution of the Greenland ice sheet based on MIROC5 RCP 8.5 climate data (a). Coloured lines indicate the different employed grid-resolutions while the individual scenarios are indicated with different line styles. The mass loss trends are corrected with the control run (projection-control) relative to the reference time. The grey shaded box shows the historical period. (b) Zoom to the RCP8.5-Rlow/med/high/none scenarios. (c) Zoom to the OO-Rmed/high scenarios.

until the end of this century is simulated, indicating accelerating mass loss for a high-emission scenario. For the RCP8.5-Rmed the mass loss reaches about 125.3 mm in 2100 (mean over G4000, G2000, G1000 and G750 results). The uncertainty quantification in the oceanic forcing results in a mean sea-level contribution, that is 7.1% less and 5.4% greater for the RCP8.5-

https://doi.org/10.5194/tc-2019-329
Preprint. Discussion started: 14 January 2020

Rlow and RCP8.5-Rhigh scenarios, respectively. When no calving front retreat is at play, i.e. the RCP8.5-Rnone scenario, the projected mean mass loss is approx. 105.0 mm, i.e ∼20 mm less compared to RCP8.5-Rmed. In contrast, the mean mass loss is considerably reduced to 26 mm and 37 mm in the OO-Rmed and OO-Rhigh experiment, respectively. Interestingly, a linear superposition of RCP8.5-Rnone and OO-Rmed leads to an overestimated mass loss of about 4.1% for G4000 and 5.3% for G750 compared to RCP8.5-Rmed where both external forcings are simultaneously at play; a linear superposition of RCP8.5-Rnone and OO-Rhigh leads to 4.5% and 5.8% overestimation. This is inline with earlier studies where this effect was already reported (Goelzer et al., 2013; Fürst et al., 2015)

Among all future projections a resolution-dependent impact on sea-level contribution is generally small compared the total signal for our grids. In 2100, the spread in sea-level contribution is 6.4 mm in RCP8.5-Rhigh, 4.1 mm in RCP8.5-Rmed, 1.5 mm in RCP8.5-Rlow and 5 mm in RCP8.5-Rnone. Merely the OO-Rlow/med scenarios exhibits a spread of 10.7 mm and 13.6 mm, respectively, which is in the order of the absolute magnitude. A notable feature for all conducted simulations is, that the the sea-level contribution in each individual experiment converges with increasing resolution.

Figure 7 summarizes the qualitative behaviour of each experiment as function of grid resolution. Note that the sea-level contribution in each experiment is normalized by its maximum. The finer resolutions tend to produce more mass loss in 2100 except for the RCP8.5-Rnone experiment, but an inverse behaviour is determined for the RP8.5-Rnone experiment. The RCP8.5-Rnone and OO-Rmed/high experiments unveil a linear behaviour as a function of grid size with regression slopes of $m = 1.50\,\mathrm{mm\,km^{-1}}$, $m = -3.27\,\mathrm{mm\,km^{-1}}$, and $m = -4.18\,\mathrm{mm\,km^{-1}}$ respectively. The trend in the full RCP8.5-Rlow/med/high scenarios is not consistent: RCP8.5-Rmed and RCP8.5-Rhigh show a peak in mass loss at the finest resolution, whereby a peak in mass loss is detected in the G2000 simulation for RCP8.5-Rlow. For the latter, it is worth to mention that the variations across the different grid simulations are lesser than 1.2%. However, an intriguing effect of the conducted simulations remains the opposite behaviour of the RCP8.5-Rnone and e.g. RCP8.5-Rhigh scenarios. In the following section, we study this effect by analysing the mass partition to get a more in-depth insight into the role of atmospheric and oceanic forcing on grid-resolution.

However, taking into account the inverse grid-dependent behaviour of the RCP8.5-Rnone and OO-Rlow/high scenarios, the combined scenarios demonstrate the competing tendencies of SMB and dynamic contribution. In a particular case, the sea-level contribution is maximized for an intermediate resolution. These competing trends seem to corroborate with results by Aschwanden et al. (2019), where an intermediate resolution reveals the largest sea-level contribution.

4.3 Mass partitioning

The relative mass loss partitioning in 2100 is shown in Fig. 8 to explore the role of the grid resolution in each experiment. The bars indicate the relative importance to sea-level contribution of ice dynamic changes in our projections. The dynamic contribution is calculated as the residual of the total mass change and the integrated SMB anomaly. The remainder explains the part of SMB. The overall picture reveals that for experiments that include the atmospheric forcing the SMB anomaly is the governing forcing regardless of the grid resolutions. However, the importance of the dynamic contribution increases with larger prescribed retreat rates of outlet glaciers; i.e. G750 with RCP8.5-Rhigh on the upper end shows the highest importance

https://doi.org/10.5194/tc-2019-329
Preprint. Discussion started: 14 January 2020

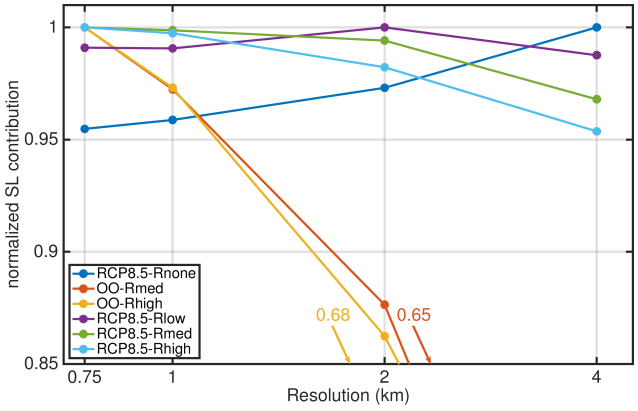

Figure 7. Projected sea-level contribution in 2100 of the Greenland ice sheet as function of the horizontal grid size. Values are normalized to the maximum of each experiment. Note the logarithmic scale of the x-axis.

of dynamic contribution with up to ∼28.4%. On the lower end, the RCP8.5-Rnone shows diminished importance of dynamic contribution (<5%). In the OO-Rmed/high scenarios, the mass loss is dominated by dynamic contribution. Concerning the grid resolution, the importance is on an equal level and exceeds 100%. The negative importance of SMB stems from the fact that the glacier retreat is cutting off regions at the ice sheet margin where the static SMB is low.

In the full experiments RCP8.5-Rlow/med/high, an increase in resolution enhances the importance of dynamic contribution. For the G750 simulation it is ∼3, 5 and 6% higher for RCP8.5-Rlow/med/high, respectively, compared to G4000. Curiously, the opposite behaviour is observed for the RCP8.5-Rnone experiment, where a finer resolution damps the importance of dynamic contribution; G4000 yield 4.9% whereby G750 2.9% dynamic contribution.

The simulated inverse grid-resolution responses raise the question of the driving causes. Overall the time series of the SMB show a decline and only minor differences among the grid resolutions (Fig. 9a). At the end of the projection, the cumulative SMB is 2.1% and 2.6% lower in the G4000 simulation for RCP8.5-Rnone and RCP8.5-Rhigh, respectively, compared to G750. These differences could be explained by different evolution of ablation areas at the margin and the SMB height-elevation feedback, in particular, affected by the control run, among all grid-resolution setups. In contrast, the cumulative ice discharge for these settings reveals an opposing response in the RCP8.5-Rnone and RCP8.5-Rhigh scenarios and more pronounced relative differences between the grid resolutions (Fig. 9b and c). At least for G2000, G1000, and G750, the ice discharge in the RCP8.5-Rnone experiment decreases over the century; the decrease in G4000 is offset by a few decades and exhibits early in the century an increase. These reductions explains the grid-dependence of the dynamic contribution as listed in the previous paragraph (RCP8.5-Rnone in Fig. 8). For RCP8.5-Rhigh, the ice discharge shows an increase consistently but is more enhanced in the finer resolutions. This finding corroborates with the grid-dependent increase of the relative ice discharge importance (RCP8.5-Rhigh in Fig. 8). As the opposing differences in RCP8.5-Rnone and RCP8.5-Rhigh are prevailing in ice discharge, it can be concluded that the ice dynamical response is a decisive factor here. The involved feedback are further explored by focusing on particular outlet glaciers in the next section.

https://doi.org/10.5194/tc-2019-329
Preprint. Discussion started: 14 January 2020

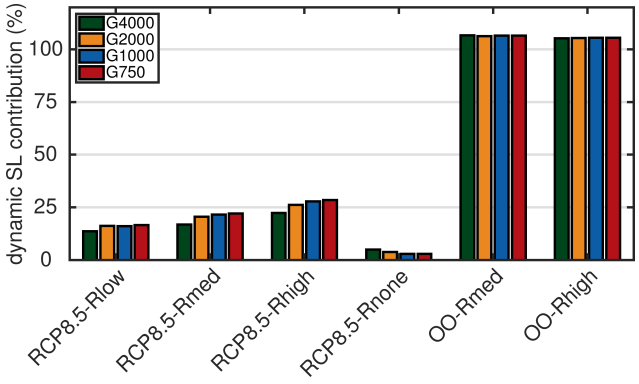

Figure 8. Mass loss partitioning for the conducted experiments. The bars indicate the relative dynamic sea-level contribution, calculated as the residual of total the mass change and the integrated SMB anomaly. The dynamic residual is a composition of front retreat and dynamic response.

However, our grid-dependent results under atmospheric only forcing correlates with the finding in Goelzer et al. (2018, Fig. 1) and the Exp. C2 in Greve and Herzfeld (2013, Figs. 7a and b therein). Interestingly, the causes for the same behaviour seem to have different origins. In Goelzer et al. (2018) the effect is likely due to an overestimated ablation area (see also Goelzer et al., 2019), whereby in our study the effect is attributed to the dynamic response of the ice sheet. The cause for the grid-dependent behaviour in Greve and Herzfeld (2013) is not specified further. Still, it is worth to mention that they report a much better agreement of simulated to observed surface velocities by increasing the resolution. A drawback in our RCP8.5-Rnone study is certainly, that the calving front remains fixed in space and time, so that outlet glaciers are hindered from adjusting freely to topographic changes.

Our experiments with considered retreat of outlet glaciers could not be compared to the additional scenarios S1, M2 and R8 experiments in Greve and Herzfeld (2013). On the one hand the external forcing approach differs and on the other hand a grid-dependent behaviour in Greve and Herzfeld (2013) is not clear (except for the enhanced sliding experiment S1, where the higher resolution setups show a higher response).

4.4 Outlet glacier response

The fact that the centennial mass loss for the full experiments increases as the grid size reduce raises the question whether this is caused by ice dynamics alone, dominant feedback with surface mass balance or the retreat, or other not obvious factors come into play. We conduct an in-depth analysis of numerous prominent outlet glaciers at GrIS (Fig. S3 and table with analysis provided as seperate SI). The general picture reveals the deduced grid-dependent behaviour, i.e. higher resolutions cause an enhanced discharge. This is illustrated in Fig. 10a for Helheim Glacier. However, this behaviour could not be adopted to all selected outlet glaciers. The presented example demonstrates that the bed topography deviates significantly among the different grid-resolutions. Generally, the bed topography of the coarser resolution is located above the bed from the finer resolution. This topographic effect is restricted to narrow confined outlet glaciers that obey a characteristic width in the order

https://doi.org/10.5194/tc-2019-329
Preprint. Discussion started: 14 January 2020

The Cryosphere Discussions
Open Access
EGU

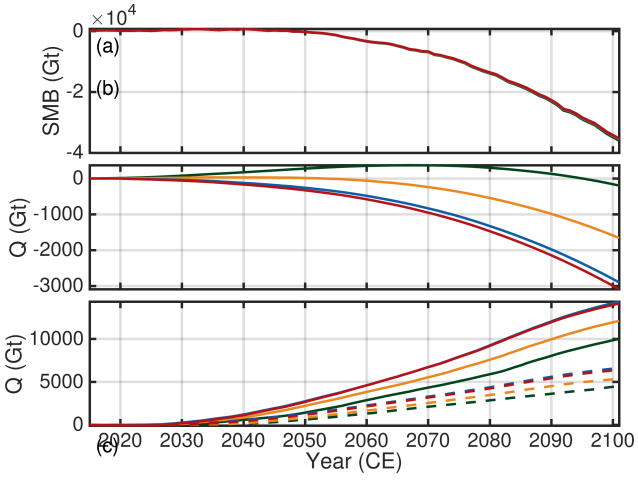

Figure 9. Time series of cumulative SMB anomaly and cumulative ice discharge Q. Colour scheme is as in previous figures. (a,b) RCP8.5-Rnone. (c) Ice discharge for RCP8.5-Rhigh (solid lines) and RCP8.5-Rlow (dashed lines). Cumulative SMB anomaly for RCP8.5-Rhigh and RCP8.5-Rlow is qualitatively similar to RCP8.5-Rnone. Ice discharge is not corrected with the control run.

of a few kilometres. Outlet glaciers that have a larger characteristic width, such as Humboldt glacier, reveal in our setups a comparable bed topography. Theses glaciers seem to have a qualitatively equal behaviour for glacier speed-up and change in ice discharge for all employed grid resolutions (Fig. 10b). This analysis demonstrates that adjacent glaciers that experience similar environmental conditions may behave differently because ice discharge is strongly controlled by glacier geometry.

The grid-dependent behaviour is highly connected to the bed topography. To study whether the response behaviour is an effect by purely reducing the grid size, we repeated the OO-Rhigh and RCP8.5-Rhigh experiments with a G1000 simulation that uses re-gridded bed topography and friction coefficient from the G4000 initial state (not shown). Projected sea-level contributions by this setups are closer to the G4000 simulation and therefore demonstrate the reduction of sea-level contribution by omitting detailed information from higher resolution. Consequently, these simulations confirm that in our setup a driving mechanism for the grid-dependent behaviour stems from additional information in the input data.

Glaciers that are converted from a marine terminating to a land terminating glacier by retreating out of the water build an own class. These glaciers are no longer subject of the retreat and show a collapse in ice discharge regardless of the grid resolution as illustrated for Store Glacier in Fig. 10c. The qualitative behaviour of the retreat seems to be similar as reported in Aschwanden et al. (2019, Fig. 4b therein), but the timing of the retreat is different. In our study, Store is unstable and retreats within this century out of the water, while in Aschwanden et al. (2019) Store Glacier is in a very stable position; the quick retreat sets in far beyond 2100 once the glacier loses contact with the bedrock high. This different response is related to the employed retreat parametrization that lacks information of the bedrock topography, such as topographic highs and lows.

For the scenarios with considered outlet glacier retreat, the induced surface lowering and frontal perturbations cause larger thinning rates and glacier acceleration; together an increase in ice discharge. The transient evolution reveals that thinning an acceleration have a larger imprint in the finer resolution by propagating faster and further upstream in the inland. The higher

https://doi.org/10.5194/tc-2019-329
Preprint. Discussion started: 14 January 2020

signal propagation rates may have additional consequences on longer time scales as the surface melt is amplified by the positive surface mass balance-elevation feedback exposing the ice surface to higher air temperatures.

The distinct slow-down in RCP8.5-Rnone is reflected in the outlet glacier response as illustrated in Fig. 10d for Store glacier. Still visible is the larger slow-down of the higher resolutions. We attribute this different response to the changing driving stress approximated as $\tau_d = \varrho_i g h |\mathrm{grad} z_s|$ (Fig. S18). Compared to 2015, the driving stress has decreased slightly more in the higher resolution in 2100 (e.g., north-western margin); or even show an opposite trend (e.g., south-eastern margin). However, the changed driving stress interact with adjusted nasal drag. The effect of resolution influences the sliding velocity in a twofold way: inversions for each resolution setup result in different k^2, as the geometric component in N differs with resolution. By analysing atmospheric only simulations (RCP8.5-Rnone) we find that the evolution of SMB, results in a larger reduction in N and τ_b, as well as decreasing sliding velocity for higher resolutions. In all scenarios, nearly all glaciers respond to lower N with higher resolutions. The change in driving stress is potentially responsible for the strong variation in τ_b. However, this needs further investigation. Beside these competing stresses, find that the change in τ_b and τ_d is very pronounced in and around the main trunks (see Fig. S17 and 18). This exemplifies the need for resolving the shear margins particularly high, which we have not accomplished in this study.

5 Discussion

The simulations conducted here reveal a spread in the RCP8.5-Rlow and RCP8.5-Rhigh scenarios ranging between 1.2 and 5.3%. The surface mass balance-elevation feedback (Eq. 4) recognized as an important mechanism accounts for an additional sea-level contribution of about 6-8% (Goelzer et al., 2020) which is of comparable magnitude. A feedback that we have not considered, but likely cause further increase in sea-level contribution and associated grid-dependent spread, is the enhanced surface melt influencing the basal conditions. Subglacial hydrology model have shown the localised effect on N, which is likely having consequences on the spread between the employed grid resolutions (e.g. Werder et al., 2013; de Fleurian et al., 2016; Sommers et al., 2018; Beyer et al., 2018).

The inferred basal friction coefficient k^2 applies to basal properties for the present-day state, and its distribution is driven by our capability to have a decent distribution of N, as the inversion strongly affected by that. Given that we rely on the parameterisation $N = \varrho_i\, g\, h + \min(0, \varrho_\mathrm{w}\, g\, z_\mathrm{b})$, we may suppress dynamic responses and a reorganization of basal conditions (in either way). That might explain the frequently detected behaviour, that velocities at retreating glacier fronts remain at a similar level. This can be overcome only with an adequate subglacial hydrology model, even if not considering seasonality. In this study, we performed the inversions for basal parameters for each grid resolution individually, which resulted in significantly different k^2 in many glacier basins. This different spatial pattern is an additional contribution to the grid dependence of the simulations. In future studies, it is worth to investigate this influence isolated. Also other studies highlight the effect of sliding on sea-level projections (e.g. Brondex et al., 2019), underpinning the importance of this mechanism.

However, our grid-dependent estimates of sea-level contribution converges around $\mathrm{RES}_\mathrm{min} \leq 1\,\mathrm{km}$. This value corroborates with Aschwanden et al. (2016) for capturing outlet glacier behaviour indicating an upper limit for horizontal grid resolution.

https://doi.org/10.5194/tc-2019-329
Preprint. Discussion started: 14 January 2020

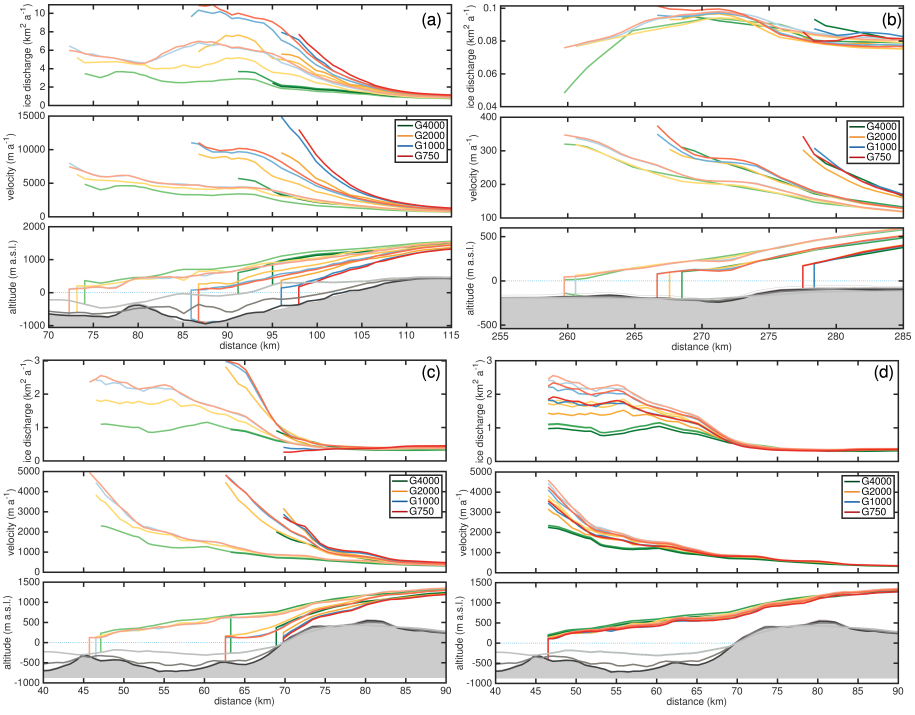

Figure 10. Response of outlet glaciers. Colour scheme is the same as in previous figures and light to dark colours indicate the years 2015, 2070 and 2100. (a) Helheim Glacier under RCP8.5-Rhigh forcing. (b) Humboldt Glacier under RCP8.5-Rhigh forcing. (c) Store Glacier under RCP8.5-Rhigh forcing. (d) Store Glacier under RCP8.5-Rnone forcing. Upper rows show the transient behaviour of the ice discharge q, the middle rows the surface velocity v and lower rows the evolution of the ice geometry. In the lower rows, the grey shaded area depicts the bedrock topography from the G750 simulation. The grey lines from dark to light indicate the bedrock topography from the G1000, G2000 and G4000 simulation. Ice discharge and geometry is not corrected with the control run.

Although we have already a decent resolution in G750, we recognise, that in many of the narrow fjords, the resolution is still insufficient, as shear margins are becoming in numerous cases subgrid phenomena. This may be a reason for under-representing glacier velocities inside the main trunk and over-estimate velocities outside the main flow as apparent in G750. This effect shall be addressed in further studies, in which ideally error estimators as presented by dos Santos et al. (2019) are engaged.

It would be most interesting to evaluate the effect the ocean does have on mass loss in general, assessing the importance of it. In our opinion, such an assessment needs to be based on simulations that represent the current dynamics of the glaciers particularly well, as the outcome depends on the capability of the model to capture the real dynamic response. Given that many of outlet glaciers exhibit lower velocities in the main trunk than observed, we thus do not draw any conclusion on the impact and importance of oceanic induced ablation versus SMB, as we lack significant feedback mechanisms (e.g., seasonal lubrication and its evolution until 2100).

https://doi.org/10.5194/tc-2019-329
Preprint. Discussion started: 14 January 2020

The floating tongues of Ryder Glacier, Petermann Glacier and Nioghalvsfjersbræ are thinning to the minimum thickness. They would retreat further, if not forced to their positions by the retreat method applied here. This may limit acceleration, and consequently, our simulations likely miss a speed-up caused by the loss of the exerted buttressing of these floating tongues.

6 Conclusions

We applied the three-dimensional finite-element higher-order model ISSM to the Greenland ice sheet to simulate the future response under climatic changes specified by the ISMIP6 protocol. The sensitivity of mass changes to the spatial resolution is tested by employing four different grids with varying horizontal resolution ranging from 4 to 0.75 km at fast-flowing outlet glaciers. The simulations reveal up to $\sim$5.3% more sea-level rise compared to the coarser resolution in the full scenario RCP8.5-Rhigh and $\sim$3.2% for RCP8.5-Rmed. In scenarios where a change in SMB is omitted, and only outlet glacier retreat is at play, the finer resolutions produce significantly more mass loss (up to 33%). When no retreat is enforced, the sensitivity of the grid-dependence exhibits an inverse behaviour, i.e. the coarser resolutions produce more mass loss. This finding is important to recognise for ice sheet models that have SMB as the dominant mass loss driver.

An apparent behaviour at many but not all individual outlet glaciers is the spread of thinning and acceleration farther inland with higher resolution. This, in turn, leads to higher ice discharge and mass transport from the interior to the ocean. The identified key mechanism that is affected by resolution is sliding, as the friction coefficient k^2 (even if static), the effective pressure N and the basal drag τ_b interact individually with the bedrock topography. In general, a reduction of N is overcompensated by a reduction in τ_b, leading to an increase in sliding speed. This study does not include an effect of increased availability of water due to increasing surface melt, thus no lubrication effect, at all. Taking this into account in future studies is important, and it may alter our findings.

Given the strong interaction of the bedrock topography with sliding, it is obvious, that the major outlet glacier should be surveyed with the latest radar technology to obtain a substantially improved survey of the base, the area of expected retreat and connected areas further upstream. This, in turn, requires ice sheet models ready to resolve these areas in grids and physics adequately.

Code and data availability. Re-gridded results at 1 km resolution will be made available in the CMIP6 archive through the Earth System Grid Federation (ESGF) with digital object identifier https://doi.org/xxx. This applies for the G1000 and G750 contributions to ISMIP6-Greenland (AWI-ISSM2 and AWI-ISSM3, respectively); all results on the native grid are available upon request to the authors. The forcing datasets are available through the ISMIP6 wiki and are also made publicly available via https://doi.org/xxx. The ice flow model ISSM is open source and freely available at https://issm.jpl.nasa.gov/ (last access: December 30, 2019), (Larour et al., 2012).

Author contributions. MR conducted the study supported by the other authors. MR set up the ISSM model and ran the experiments. AH analysed the results for the individual glaciers. HG calculated the retreat masks. MR wrote the manuscript together with the other authors.

https://doi.org/10.5194/tc-2019-329
Preprint. Discussion started: 14 January 2020

Competing interests. The authors declare that they have no conflict of interest.

Acknowledgements. We thank the Climate and Cryosphere (CliC) effort, which provided support for ISMIP6 through sponsoring of workshops, hosting the ISMIP6 website and wiki, and promoted ISMIP6. We acknowledge the World Climate Research Programme, which, through its Working Group on Coupled Modelling, coordinated and promoted CMIP5 and CMIP6. We thank the climate modeling groups for producing and making available their model output, the Earth System Grid Federation (ESGF) for archiving the CMIP data and providing access, the University at Buffalo for ISMIP6 data distribution and upload, and the multiple funding agencies who support CMIP5 and CMIP6 and ESGF. We thank the ISMIP6 steering committee, the ISMIP6 model selection group and ISMIP6 dataset preparation group for their continuous engagement in defining ISMIP6 and all their efforts.

Martin Rückamp acknowledges support of the Helmholtz Climate Initiative REKLIM (Regional Climate Change). Heiko Goelzer has received funding from the programme of the Netherlands Earth System Science Centre (NESSC), financially supported by the Dutch Ministry of Education, Culture and Science (OCW) under grant no. 024.002.001.

We thank Thomas Kleiner (AWI) and Ralf Greve (ILTS) for continuous and fruitful discussions on simulations. We would like to thank Natalja Rakowsky, Malte Thoma and Bernadette Fritzsch for maintaining excellent computing facilities at AWI and DKRZ. The high-resolution simulations were run on the DKRZ HPC system Mistral under grant ab1073. We also acknowledge the outstanding support of the ISSM team.

https://doi.org/10.5194/tc-2019-329
Preprint. Discussion started: 14 January 2020

References

Aschwanden, A., Fahnestock, M. A., and Truffer, M.: Complex Greenland outlet glacier flow captured, Nat. Commun., 7, 10 524, https://doi.org/10.1038/ncomms10524, 2016.

Aschwanden, A., Fahnestock, M. A., Truffer, M., Brinkerhoff, D. J., Hock, R., Khroulev, C., Mottram, R., and Khan, S. A.: Contribution of the Greenland Ice Sheet to sea level over the next millennium, Science Advances, 5, https://doi.org/10.1126/sciadv.aav9396, 2019.

Barthel, A., Agosta, C., Little, C. M., Hatterman, T., Jourdain, N. C., Goelzer, H., Nowicki, S., Seroussi, H., Straneo, F., and Bracegirdle, T. J.: CMIP5 model selection for ISMIP6 ice sheet model forcing: Greenland and Antarctica, The Cryosphere Discussions, 2019, 1–34, https://doi.org/10.5194/tc-2019-191, 2019.

Beckmann, A. and Goosse, H.: A parameterization of ice shelf-ocean interaction for climate models, Ocean Modelling, 5, 157–170, https://doi.org/10.1016/S1463-5003(02)00019-7, 2003.

Beyer, S., Kleiner, T., Aizinger, V., Rückamp, M., and Humbert, A.: A confined–unconfined aquifer model for subglacial hydrology and its application to the Northeast Greenland Ice Stream, The Cryosphere, 12, 3931–3947, https://doi.org/10.5194/tc-12-3931-2018, https://www.the-cryosphere.net/12/3931/2018/, 2018.

Bindschadler, R. A., Nowicki, S., Abe-Ouchi, A., Aschwanden, A., Choi, H., Fastook, J., Granzow, G., Greve, R., Gutowski, G., Herzfeld, U. C., Jackson, C., Johnson, J., Khroulev, C., Levermann, A., Lipscomb, W. H., Martin, M. A., Morlighem, M., Parizek, B. R., Pollard, D., Price, S. F., Ren, D., Saito, F., Sato, T., Seddik, H., Seroussi, H., Takahashi, K., Walker, R., and Wang, W. L.: Ice-sheet model sensitivities to environmental forcing and their use in projecting future sea level (the SeaRISE project), J. Glaciol., 59, 195–224, https://doi.org/10.3189/2013JoG12J125, 2013.

Blatter, H.: Velocity and stress fields in grounded glaciers: a simple algorithm for including deviatoric stress gradients, J. Glaciol., 41, 333–344, https://doi.org/10.3189/S002214300001621X, 1995.

Bondzio, J. H., Morlighem, M., Seroussi, H., Kleiner, T., Rückamp, M., Mouginot, J., Moon, T., Larour, E. Y., and Humbert, A.: The mechanisms behind Jakobshavn Isbræ's acceleration and mass loss: A 3-D thermomechanical model study, Geophys. Res. Lett., 44, 6252–6260, https://doi.org/10.1002/2017GL073309, 2017.

Brondex, J., Gillet-Chaulet, F., and Gagliardini, O.: Sensitivity of centennial mass loss projections of the Amundsen basin to the friction law, The Cryosphere, 13, 177–195, https://doi.org/10.5194/tc-13-177-2019, https://www.the-cryosphere.net/13/177/2019/, 2019.

Choi, Y., Morlighem, M., Rignot, E., Mouginot, J., and Wood, M.: Modeling the Response of Nioghalvfjerdsfjorden and Zachariae Isstrøm Glaciers, Greenland, to Ocean Forcing Over the Next Century, Geophysical Research Letters, 44, 11,071–11,079, https://doi.org/10.1002/2017GL075174, 2017.

Church, J. A., Clark, P. U., Cazenave, A., Gregory, J. M., Jevrejeva, S., Levermann, A., Merrifield, M., Milne, G., Nerem, R., Nunn, P., et al.: Sea level change, in: Climate Change 2013: The Physical Science Basis. Working Group I Contribution to the Fifth Assessment Report of the Intergovernmental Panel on Climate Change, pp. 1137–1216, Cambridge University Press, 2013.

Cogley, J., Hock, R., Rasmussen, L., Arendt, A., Bauder, A., Braithwaite, R., Jansson, P., Kaser, G., Möller, M., Nicholson, L., and Zemp, M.: Glossary of Glacier Mass Balance and Related Terms, Tech. Rep. 86, IHP-VII Technical Documents in Hydrology, UNESCO-IHP, Paris, 2011.

https://doi.org/10.5194/tc-2019-329
Preprint. Discussion started: 14 January 2020

de Fleurian, B., Morlighem, M., Seroussi, H., Rignot, E., van den Broeke, M. R., Kuipers Munneke, P., Mouginot, J., Smeets, P. C. J. P., and Tedstone, A. J.: A modeling study of the effect of runoff variability on the effective pressure beneath Russell Glacier, West Greenland, Journal of Geophysical Research: Earth Surface, 121, 1834–1848, https://doi.org/10.1002/2016JF003842, 2016.

dos Santos, T. D., Morlighem, M., Seroussi, H., Devloo, P. R. B., and Simões, J. C.: Implementation and performance of adaptive mesh refinement in the Ice Sheet System Model (ISSM v4.14), Geoscientific Model Development, 12, 215–232, https://doi.org/10.5194/gmd-12-215-2019, 2019.

Enderlin, E. M., Howat, I. M., Jeong, S., Noh, M.-J., Angelen, J. H., and Broeke, M. R.: An improved mass budget for the Greenland ice sheet, Geophysical Research Letters, 41, 866–872, https://doi.org/10.1002/2013GL059010, 2014.

Ettema, J., van den Broeke, M. R., van Meijgaard, E., van de Berg, W. J., Bamber, J. L., Box, J. E., and Bales, R. C.: Higher surface mass balance of the Greenland ice sheet revealed by high-resolution climate modeling, Geophysical Research Letters, 36, n/a–n/a, https://doi.org/10.1029/2009GL038110, l12501, 2009.

Eyring, V., Bony, S., Meehl, G. A., Senior, C. A., Stevens, B., Stouffer, R. J., and Taylor, K. E.: Overview of the Coupled Model Intercomparison Project Phase 6 (CMIP6) experimental design and organization, Geoscientific Model Development, 9, 1937–1958, https://doi.org/10.5194/gmd-9-1937-2016, 2016.

Fettweis, X., Box, J. E., Agosta, C., Amory, C., Kittel, C., Lang, C., van As, D., Machguth, H., and Gallée, H.: Reconstructions of the 1900–2015 Greenland ice sheet surface mass balance using the regional climate MAR model, The Cryosphere, 11, 1015–1033, https://doi.org/10.5194/tc-11-1015-2017, 2017.

Fettweis, X., Fettweis, X., Hofer, S., Krebs-Kanzow, U., Amory, C., Aoki, T., Berends, C. J., Born, A., Box, J. E., Delhasse, A., Fujita, K., Gierz, P., Goelzer, H., Hanna, E., Hashimoto, A., Huybrechts, P., Kapsch, M.-L., King, M. D., Kittel, C., Lang, C., Langen, P. L., Lenaerts, J. T. M., Liston, G. E., Lohmann, G., Mernild, S. H., Mikolajewicz, U., Modali, K., Mottram, R. H., Niwano, M., Noël, B., Ryan, J. C., Smith, A., Streffing, J., Tedesco, M., Berg, W. J. v. d., Broeke, M. v. d., Wal, R. S. W. v. d., Kampenhout, L. v., Wilton, D., Wouters, B., Ziemen, F., and Zolles, T.: GrSMBMIP: Intercomparison of the modelled 1980-2012 surface mass balance over the Greenland Ice sheet, The Cryopshere, submitted, 2020.

Franco, B., Fettweis, X., Lang, C., and Erpicum, M.: Impact of spatial resolution on the modelling of the Greenland ice sheet surface mass balance between 1990–2010, using the regional climate model MAR, The Cryosphere, 6, 695–711, https://doi.org/10.5194/tc-6-695-2012, 2012.

Fürst, J. J., Goelzer, H., and Huybrechts, P.: Ice-dynamic projections of the Greenland ice sheet in response to atmospheric and oceanic warming, The Cryosphere, 9, 1039–1062, https://doi.org/10.5194/tc-9-1039-2015, 2015.

Gillet-Chaulet, F., Gagliardini, O., Seddik, H., Nodet, M., Durand, G., Ritz, C., Zwinger, T., Greve, R., and Vaughan, D. G.: Greenland ice sheet contribution to sea-level rise from a new-generation ice-sheet model, Cryosphere, 6, 1561–1576, https://doi.org/10.5194/tc-6-1561-2012, 2012.

Goelzer, H., Huybrechts, P., Fürst, J., Nick, F., Andersen, M., Edwards, T., Fettweis, X., Payne, A., and Shannon, S.: Sensitivity of Greenland Ice Sheet Projections to Model Formulations, Journal of Glaciology, 59, 733–749, https://doi.org/10.3189/2013JoG12J182, 2013.

Goelzer, H., Nowicki, S., Edwards, T., Beckley, M., Abe-Ouchi, A., Aschwanden, A., Calov, R., Gagliardini, O., Gillet-Chaulet, F., Golledge, N. R., Gregory, J., Greve, R., Humbert, A., Huybrechts, P., Kennedy, J. H., Larour, E., Lipscomb, W. H., Le clec'h, S., Lee, V., Morlighem, M., Pattyn, F., Payne, A. J., Rodehacke, C., Rückamp, M., Saito, F., Schlegel, N., Seroussi, H., Shepherd, A., Sun, S., van de Wal, R., and Ziemen, F. A.: Design and results of the ice sheet model initialisation experiments initMIP-Greenland: an ISMIP6 intercomparison, Cryosphere, 12, 1433–1460, https://doi.org/10.5194/tc-12-1433-2018, 2018.

https://doi.org/10.5194/tc-2019-329
Preprint. Discussion started: 14 January 2020

555 Goelzer, H., Noel, B. P. Y., Edwards, T. L., Fettweis, X., Gregory, J. M., Lipscomb, W. H., van de Wal, R. S. W., and van den Broeke, M. R.: Remapping of Greenland ice sheet surface mass balance anomalies for large ensemble sea-level change projections, The Cryosphere Discussions, 2019, 1–20, https://doi.org/10.5194/tc-2019-188, 2019.

Goelzer, H., Nowicki, S., Payne, A., Larour, E., Seroussi, H., Lipscomb, W. H., Gregory, J., Abe-Ouchi, A., Shepherd, A., Simon, E., Agosta, C., Alexander, P., Aschwanden, A., Barthel, A., Calov, R., Chambers, C., Choi, Y., Cuzzone, J., Dumas, C., Edwards, T., Felikson, D., 560 Fettweis, X., Golledge, N. R., Greve, R., Humbert, A., Huybrechts, P., clec'h, S. L., Lee, V., Leguy, G., Little, C., Lowry, D. P., Morlighem, M., Nias, I., Quiquet, A., Rückamp, M., Schlegel, N.-J., Slater, D., Smith, R., Straneo, F., Tarasov, L., van de Wal, R., , and van den Broeke, M.: The future sea-level contribution of the Greenland ice sheet: a multimodel ensemble study of ISMIP6, The Cryopshere, submitted, 2020.

Greve, R.: Relation of measured basal temperatures and the spatial distribution of the geothermal heat flux for the Greenland ice sheet, 565 Annals of Glaciology, 42, 424–432, 2005.

Greve, R. and Herzfeld, U. C.: Resolution of ice streams and outlet glaciers in large-scale simulations of the Greenland ice sheet, Ann. Glaciol., 54, 209–220, https://doi.org/10.3189/2013AoG63A085, 2013.

Joughin, I., Smith, B., Howat, I., Scambos, T., and Moon, T.: Greenland flow variability from ice-sheet-wide velocity mapping, J. Glaciol., 56, 415–430, https://doi.org/10.3189/002214310792447734, 2010.

570 Joughin, I., Smith, B., Howat, I., and Scambos, T.: MEaSUREs Multi-year Greenland Ice Sheet Velocity Mosaic, Version 1. Boulder, Colorado USA. NASA National Snow and Ice Data Center Distributed Active Archive Center., 2016.

Larour, E., Seroussi, H., Morlighem, M., and Rignot, E.: Continental scale, high order, high spatial resolution, ice sheet modeling using the Ice Sheet System Model (ISSM), J. Geophys. Res. Earth Surf., 117, F01 022, https://doi.org/10.1029/2011JF002140, 2012.

Moon, T., Joughin, I., Smith, B., and Howat, I.: 21st-Century Evolution of Greenland Outlet Glacier Velocities, Science, 336, 576–578, 575 https://doi.org/10.1126/science.1219985, 2012.

Morlighem, M., Rignot, E., Seroussi, H., Larour, E., Dhia, H. B., and Aubry, D.: Spatial patterns of basal drag inferred using control methods from a full-Stokes and simpler models for Pine Island Glacier, West Antarctica, Geophysical Research Letters, 37, https://doi.org/10.1029/2010GL043853, 2010.

Morlighem, M., Williams, C. N., Rignot, E., An, L., Arndt, J. E., Bamber, J. L., Catania, G., Chauché, N., Dowdeswell, J. A., Dorschel, B., 580 Fenty, I., Hogan, K., Howat, I., Hubbard, A., Jakobsson, M., Jordan, T. M., Kjeldsen, K. K., Millan, R., Mayer, L., Mouginot, J., Noël, B. P. Y., O'Cofaigh, C., Palmer, S., Rysgaard, S., Seroussi, H., Siegert, M. J., Slabon, P., Straneo, F., van den Broeke, M. R., Weinrebe, W., Wood, M., and Zinglersen, K. B.: BedMachine v3: Complete bed topography and ocean bathymetry mapping of Greenland from multibeam echo sounding combined with mass conservation, Geophys. Res. Lett., 44, 11 051–11 061, https://doi.org/10.1002/2017GL074954, 2017.

585 Moss, R. H., Edmonds, J. A., Hibbard, K. A., Manning, M. R., Rose, S. K., van Vuuren, D. P., Carter, T. R., Emori, S., Kainuma, M., Kram, T., Meehl, G. A., Mitchell, J. F. B., Nakicenovic, N., Riahi, K., Smith, S. J., Stouffer, R. J., Thomson, A. M., Weyant, J. P., and Wilbanks, T. J.: The next generation of scenarios for climate change research and assessment, Nature, 463, 747–756, https://doi.org/10.1038/nature08823, 2010.

Mouginot, J., Rignot, E., Bjørk, A. A., van den Broeke, M., Millan, R., Morlighem, M., Noël, B., Scheuchl, B., and Wood, M.: Forty-six 590 years of Greenland Ice Sheet mass balance from 1972 to 2018, Proceedings of the National Academy of Sciences, 116, 9239–9244, https://doi.org/10.1073/pnas.1904242116, 2019.

Nerem, R. S., Beckley, B. D., Fasullo, J. T., Hamlington, B. D., Masters, D., and Mitchum, G. T.: Climate-change-driven accelerated sea-level rise detected in the altimeter era, P. Natl. Acad. Sci., 115, 2022–2025, https://doi.org/10.1073/pnas.1717312115, 2018.

Noël, B., van de Berg, W. J., van Wessem, J. M., van Meijgaard, E., van As, D., Lenaerts, J. T. M., Lhermitte, S., Kuipers Munneke, P., Smeets, C. J. P. P., van Ulft, L. H., van de Wal, R. S. W., and van den Broeke, M. R.: Modelling the climate and surface mass balance of polar ice sheets using RACMO2 – Part 1: Greenland (1958–2016), The Cryosphere, 12, 811–831, https://doi.org/10.5194/tc-12-811-2018, 2018.

Nowicki, S., Bindschadler, R. A., Abe-Ouchi, A., Aschwanden, A., Bueler, E., Choi, H., Fastook, J., Granzow, G., Greve, R., Gutowski, G., Herzfeld, U., Jackson, C., Johnson, J., Khroulev, C., Larour, E., Levermann, A., Lipscomb, W. H., Martin, M. A., Morlighem, M., Parizek, B. R., Pollard, D., Price, S. F., Ren, D., Rignot, E., Saito, F., Sato, T., Seddik, H., Seroussi, H., Takahashi, K., Walker, R., and Wang, W. L.: Insights into spatial sensitivities of ice mass response to environmental change from the SeaRISE ice sheet modeling project II: Greenland, J. Geophys. Res. Earth Surf., 118, 1025–1044, https://doi.org/10.1002/jgrf.20076, 2013.

Nowicki, S. M. J., Payne, A., Larour, E., Seroussi, H., Goelzer, H., Lipscomb, W., Gregory, J., Abe-Ouchi, A., and Shepherd, A.: Ice Sheet Model Intercomparison Project (ISMIP6) contribution to CMIP6, Geoscientific Model Development, 9, 4521–4545, https://doi.org/10.5194/gmd-9-4521-2016, 2016.

Nowicki, S. M. J., Payne, A., and co-authors: Contrasting contributions to future sea level under CMIP5 and CMIP6 scenarios from the Greenland and Antarctic ice sheets,, Geophysical Research Letters, submitted, 2020a.

Nowicki, S. M. J., Payne, A., Larour, E., Seroussi, H., Goelzer, H., Lipscomb, W., Gregory, J., A.-O. A., and Shepherd, A.: Experimental protocol for sea level projections from ISMIP6 standalone ice sheet models, Geoscientific Model Development; submitted, 2020b.

Pattyn, F.: A new three-dimensional higher-order thermomechanical ice-sheet model: basic sensitivity, ice-stream development and ice flow across subglacial lakes, J. Geophys. Res. Solid Earth, 108, 2382, https://doi.org/10.1029/2002JB002329, 2003.

Rietbroek, R., Brunnabend, S.-E., Kusche, J., Schröter, J., and Dahle, C.: Revisiting the contemporary sea-level budget on global and regional scales, P. Natl. Acad. Sci., 113, 1504–1509, https://doi.org/10.1073/pnas.1519132113, 2016.

Rückamp, M., Falk, U., Frieler, K., Lange, S., and Humbert, A.: The effect of overshooting 1.5 °C global warming on the mass loss of the Greenland Ice Sheet, Earth System Dynamics, 9, 1169–1189, https://doi.org/10.5194/esd-9-1169-2018, 2018.

Rückamp, M., Greve, R., and Humbert, A.: Comparative simulations of the evolution of the Greenland ice sheet under simplified Paris Agreement scenarios with the models SICOPOLIS and ISSM, Polar Science, https://doi.org/10.1016/j.polar.2018.12.003, in press, 2019a.

Rückamp, M., Neckel, N., Berger, S., Helm, V., and Humbert, A.: Calving induced Speedup of Petermann Glacier, Journal of Geophysical Research: Earth Surface, 124, 216–228, https://doi.org/10.1029/2018JF004775, 2019b.

Seroussi, H. and Morlighem, M.: Representation of basal melting at the grounding line in ice flow models, Cryosphere, 12, 3085–3096, https://doi.org/10.5194/tc-12-3085-2018, 2018.

Seroussi, H., Morlighem, M., Rignot, E., Khazendar, A., Larour, E., and Mouginot, J.: Dependence of century-scale projections of the Greenland ice sheet on its thermal regime, J. Glaciol., 59, 1024–1034, https://doi.org/doi:10.3189/2013JoG13J054, 2013.

Seroussi, H., Morlighem, M., Larour, E., Rignot, E., and Khazendar, A.: Hydrostatic grounding line parameterization in ice sheet models, Cryosphere, 8, 2075–2087, https://doi.org/10.5194/tc-8-2075-2014, 2014.

Shepherd, A., Ivins, E., Rignot, E., Smith, B., van den Broeke, M., Velicogna, I., Whitehouse, P., Briggs, K., Joughin, I., Krinner, G., Nowicki, S., Payne, T., Scambos, T., Schlegel, N., Geruo, A., Agosta, C., Ahlstrøm, A., Babonis, G., Barletta, V. R., Bjørk, A. A., Blazquez, A., Bonin, J., Colgan, W., Csatho, B., Cullather, R., Engdahl, M. E., Felikson, D., Fettweis, X., Forsberg, R., Hogg, A. E., Gallee, H., Gardner, A., Gilbert, L., Gourmelen, N., Groh, A., Gunter, B., Hanna, E., Harig, C., Helm, V., Horvath, A., Horwath, M., Khan, S., Kjeldsen, K. K.,

https://doi.org/10.5194/tc-2019-329
Preprint. Discussion started: 14 January 2020

Konrad, H., Langen, P. L., Lecavalier, B., Loomis, B., Luthcke, S., McMillan, M., Melini, D., Mernild, S., Mohajerani, Y., Moore, P., Mottram, R., Mouginot, J., Moyano, G., Muir, A., Nagler, T., Nield, G., Nilsson, J., Noël, B., Otosaka, I., Pattle, M. E., Peltier, W. R., Pie, N., Rietbroek, R., Rott, H., Sørensen, L. S., Sasgen, I., Save, H., Scheuchl, B., Schrama, E., Schröder, L., Seo, K.-W., Simonsen, S. B., Slater, T., Spada, G., Sutterley, T., Talpe, M., Tarasov, L., Jan van de Berg, W., van der Wal, W., van Wessem, M., Vishwakarma, B. D., Wiese, D., Wilton, D., Wagner, T., Wouters, B., Wuite, J., and Team, T. I.: Mass balance of the Greenland Ice Sheet from 1992 to 2018, Nature, https://doi.org/10.1038/s41586-019-1855-2, 2019.

Slater, D. A., Felikson, D., Straneo, F., Goelzer, H., Little, C. M., Morlighem, M., Fettweis, X., and Nowicki, S.: 21st century ocean forcing of the Greenland Ice Sheet for modeling of sea level contribution, The Cryosphere Discussions, 2019, 1–34, https://doi.org/10.5194/tc-2019-222, 2019a.

Slater, D. A., Straneo, F., Felikson, D., Little, C. M., Goelzer, H., Fettweis, X., and Holte, J.: Estimating Greenland tidewater glacier retreat driven by submarine melting, The Cryosphere, 13, 2489–2509, https://doi.org/10.5194/tc-13-2489-2019, 2019b.

Sommers, A., Rajaram, H., and Morlighem, M.: SHAKTI: Subglacial Hydrology and Kinetic, Transient Interactions v1.0, Geoscientific Model Development, 11, 2955–2974, https://doi.org/10.5194/gmd-11-2955-2018, https://www.geosci-model-dev.net/11/2955/2018/, 2018.

Werder, M. A., Hewitt, I. J., Schoof, C. G., and Flowers, G. E.: Modeling channelized and distributed subglacial drainage in two dimensions, Journal of Geophysical Research: Earth Surface, 118, 2140–2158, https://doi.org/10.1002/jgrf.20146, 2013.

Wilson, N., Straneo, F., and Heimbach, P.: Submarine melt rates and mass balance for Greenland's remaining ice tongues, Cryosphere, 11, 2773–2782, https://doi.org/10.5194/tc-11-2773-2017, 2017.